An improved regional branched GDGT-based soil temperature calibration for the Tropical Andes of Colombia: Towards a soil calibration for the tropics.

Lina C. Pérez-Angel[1,2,3,4*], Camilo Montes[5], Peter Molnar[1,2], Kathryn Snell[1], Balaji Rajagopalan[2,6], Catalina Gonzalez-Arango[7], Nadia Dildar[1,3,4], Julio Sepúlveda[1,3,4*]

[1]Department of Geological Sciences, University of Colorado Boulder, Boulder, Colorado, 80309, USA.
[2]Cooperative Institute for Research in Environmental Sciences, University of Colorado Boulder, Boulder, Colorado, 80309, USA
[3]Institute of Arctic and Alpine Research (INSTAAR), University of Colorado Boulder, Boulder, Colorado, 80309, USA
[4]Organic Geochemistry Laboratory, University of Colorado Boulder, Boulder, Colorado, 80309, USA
[5]Department of Physics and Geosciences, Universidad del Norte, Barranquilla, Colombia
[6]Department of Civil, Environmental and Architectural Engineering, University of Colorado Boulder, Boulder, Colorado, 80309, USA
[7]Department of Biological Sciences, Universidad de Los Andes, Bogotá, Colombia

Corresponding authors*: Lina C. Pérez-Angel (Lina.PerezAngel@colorado.edu); Julio Sepúlveda (jsepulveda@colorado.edu)

Key Points:

- New regional air and soil brGDGT calibrations for the Eastern Cordillera of Colombia have root-mean-square-errors of 1.1 °C and 1.2 °C, respectively.
- A soil calibration for the tropics has a root-mean-square-error of 2.2 °C, compared with global calibrations with root-mean-square-errors of 3.8 – 4.9 °C.

Abstract

Branched glycerol dialkyl glycerol tetraethers (brGDGTs) are bacterial cell membrane lipids that, when preserved in sedimentary archives, can be used to infer continental paleotemperatures from sedimentary records. Although global calibrations capture a global relationship between the distribution of brGDGTs and temperatures, they underestimate temperatures for tropical regions by ~15 °C. Furthermore, some global calibrations reach saturation at around 24-25 °C, and, in general, they have root-mean-squared errors (RMSEs ≈ ~4 °C) that are too large to resolve small variations in paleoclimate variability in tropical regions. We present a detailed regional calibration of soil brGDGTs along altitudinal transects on both flanks of the Eastern Cordillera of Colombia in the northern tropical Andes that spans ~3200 m in elevation, 17 °C in mean annual soil temperatures, and 19 °C in mean annual air temperatures. These new soil and air regional calibrations yield root-mean-square errors (RMSEs) of 1.2 °C and 1.1 °C, respectively. When combined with existing data from elsewhere in the tropics, the integrated data not only fit a calibration with an RMSE of 2.2 °C, but also fit mean annual air temperatures as high as 27.9 °C, resulting in a calibration that can be used in paleoclimate studies throughout the tropics.

Plain Language Summary

Small variations in temperatures within the tropics can have large effects on climate at mid- and high-latitudes. A common example is how the El Niño Southern Oscillation (ENSO) can alter climate around the world. Quantitative terrestrial temperature records from the tropics, however, are scarce. A new lipid-based proxy, based on the abundances of different bacterial lipids, has enabled quantitative estimates of continental temperature, but the uncertainties in these global estimates remain large (3.8-4.9 °C). Because past temperature changes in the tropics are small

relative to other regions, high-precision temperature estimates are necessary to evaluate small changes that could have bigger effects elsewhere. In this study, we generated new data from the Eastern Cordillera of Colombia to estimate air and soil temperatures using this lipid-based proxy. In order to improve temperature reconstructions within the tropics, we compiled tropical soil data to provide a calibration for this latitudinal range.

1. Introduction

Small variations in temperatures within the tropics can have large effects on climate at higher latitudes, as illustrated by teleconnections from the Eastern Tropical Pacific and the El Niño Southern Oscillation (ENSO) (e.g., Halpert and Ropelewski, 1992; Ropelewski and Halpert, 1987, 1989; Sarachik and Cane, 2010; Trenberth et al., 1998). It follows that past mid-latitude climates may also reflect, and perhaps result from, variations in tropical conditions. Most quantitative estimates of past temperature from the tropics, however, come from marine sediment (e.g., Dekens et al., 2007; Groeneveld et al., 2006; Herbert et al., 2010, 2016; Lawrence et al., 2006; Ravelo et al., 2006; Wara et al., 2005; Zachos et al., 2001). Paleoclimate records from continental regions are scarce (e.g., Salzmann et al., 2013) and, in many cases, qualitative (e.g., Hooghiemstra et al., 2006; Van der Hammen et al., 1973). Missing has been a well calibrated proxy that quantifies past temperatures and can be applied widely to past tropical environments.

Recently, lipid-based paleotemperature proxies have evolved as a tool for the quantitative reconstruction of past continental temperatures (e.g., De Jonge et al., 2014; Lu et al., 2016; Peterse et al., 2012, 2014; Thomas et al., 2017; Weijers et al., 2007; Yamammoto et al., 2016). The development of these proxies has been particularly relevant in places where rocks with preserved organic matter may not preserve other materials useful for temperature

reconstructions, such as carbonates and fossil leaves (e.g., Ghosh et al., 2006; Wolfe, 1995). To enable accurate estimates of past temperatures in tropical environments, we calibrated a lipid-based paleotemperature proxy that exploits branched glycerol dialkyl glycerol tetraethers (brGDGTs). We measured both air and soil temperatures and brGDGTs along two altitudinal transect across the Eastern Cordillera of Colombia to construct regional calibrations for each. We then incorporated published data from elsewhere in the tropics to derive a pan-tropical calibration of air temperatures.

2. Background on brGDGTs

Branched glycerol dialkyl glycerol tetraethers (brGDGTs) are cell membrane lipids (Figure 1) produced by bacteria in soils, peats, lakes, marine sediment, and anoxic water columns (Liu et al., 2010, 2012, 2014; Russell et al., 2018; Sinninghe Damsté et al., 2000; Weber et al., 2015, 2018; Weijers et al., 2006, 2007). Early studies demonstrated that the distribution of brGDGTs in soils, expressed as the cyclisation of branched tetraethers (CBT, equation 1; Weijers et al., 2007) and the methyl index of branched tetraethers (MBT, equation 2, Weijers et al., 2007), correlated with the pH of the soil and mean annual air temperature (MAAT), respectively (Weijers et al., 2007):

$$CBT = -log\frac{(Ib+IIb+IIb')}{(Ia+IIa+IIa')}, \text{ and} \quad (1)$$

$$MBT = \frac{(Ia+Ib+Ic)}{(Ia+Ib+Ic+IIa+IIa'+IIb+IIb'+IIc+IIc'+IIIa+IIIa'+IIIb+IIIb'+IIIc+IIIc')}. \quad (2)$$

Prime numerals (e.g., IIa') indicate 6-methyl isomers, which were originally not separated from 5-methyl isomers (e.g., IIa) by the chromatographic method used in Weijers et al. (2007) and later in Peterse et al. (2012), and thus not used to distinguish these isomers in the

97 original representation of indices. To be consistent with the most recent and commonly used
98 nomenclature, we distinguish between both isomers. Each term in the equations, and illustrated
99 in Figure 1, uses the fractional abundance (FA) of these molecular structures, which is the ratio
100 of the abundance of a particular brGDGT to the total number of brGDGTs in the sample. The
101 MBT index was later refined by Peterse et al. (2012), who excluded brGDGTs-IIIb, -IIIb', -IIIc,
102 and -IIIc' (Figure 1), because, in general, they are found in low abundance and below the
103 analytical limit of detection. Peterse et al. (2012) defined the MBT' as follows:

104 $$MBT' = \frac{(Ia+Ib+Ic)}{(Ia+Ib+Ic+IIa+IIa'+IIb+IIb'+IIc+IIc'+IIIa+IIIa')}. \quad (3)$$

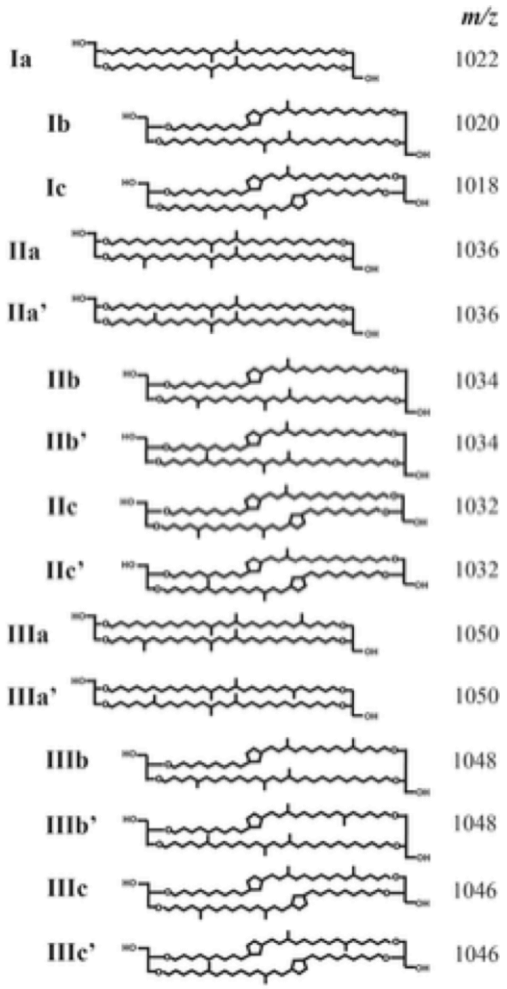

Figure 1. Chemical structures of brGDGTs used in this study. Each letter corresponds to different structure from a methyl to a cyclopentyl moiety; 'a' structures have no cyclopentyl moieties, 'b' structures have one cyclopentyl moiety, and 'c' structures have two cyclopentyl moieties. The structures with C6-methylation are referenced with a prime symbol. C5-methylations are highlighted in blue in the corresponding structure. Figure modified from Hanna et al. (2016).

When incorporated in global soil datasets and calibrations, these indices allow for the reconstruction of past soil pH and MAAT using the following relationships (Peterse et al., 2012):

$$\text{pH} = 7.90 - 1.97 \times \text{CBT} \ (n = 176, R^2 = 0.70, \text{RMSE} = 0.8), \quad (4)$$

116 $$MAAT = 0.81 - 5.67 \times CBT + 31.0 \times MBT' \ (n = 176, R^2 = 0.59, RMSE = 5.0\ °C), \quad (5)$$

117 where n is the number of samples used in the calibration, R^2 is the coefficient of determination
118 between MAAT and the combination of brGDGTs, and RMSE is the root mean square error for
119 each temperature estimate using the respective calibration.

120 More recently, using an improved chromatographic method capable of separating 5- and
121 6-methyl isomers, De Jonge et al. (2014) demonstrated that although 5-methyl brGDGTs were
122 mostly influenced by temperature, 6-methyl brGDGTs correlate with pH. By including only 5-
123 methyl brGDGTs from global datasets, De Jonge et al. (2014) produced a new methylation index
124 (MBT'_{5me}):

125 $$MBT'_{5me} = \frac{(Ia+Ib+Ic)}{(Ia+Ib+Ic+IIa+IIb+IIc+IIIa)}. \quad (6)$$

126 Then, they used this index to produce a simple linear equation that estimates MAAT,
127 independently of soil pH:

128 $$MAAT = -8.57 + 31.45 \times MBT'_{5me} \ (n = 231, R^2 = 0.64, RMSE = 4.9\ °C). \quad (7)$$

129 The MBT'_{5me} index, as all previous MBT indices, is a fraction whose maximum possible
130 value is one. When the MBT'_{5me} index reaches one ($MBT'_{5me} = 1$), Equation 7 allows for the
131 reconstruction of MAAT only up to 22.7 °C, and therefore, this equation does not allow a
132 reliable reconstruction of MAAT in tropical regions, which exceeds 22.7 °C in most regions. To
133 expand the range of temperature that can be reconstructed, De Jonge et al. (2014) proposed a
134 multiple linear regression using the fractional abundance (FA) of individual 5-methyl brGDGTs
135 (Figure 1):

136 $$MAAT_{mr} = 7.17 + 17.1 \times [Ia] + 25.9 \times [Ib] + 34.4 \times [Ic] - 28.6 \times [IIa]$$

137 $$(n = 222, R^2 = 0.68, RMSE = 4.6\ °C). \quad (8)$$

Their measurements, however, extend only to ~26 °C, and extrapolating to higher temperatures must be done with caution.

More recently, Naafs et al. (2017) refined these global calibrations by filtering samples from the dataset using the relative abundance of 6-methyl brGDGTs (IR_{6me} index) proposed by Dang et al. (2016):

$$IR_{6me} = \frac{[IIa'] + [IIb'] + [IIc'] + [IIIa'] + [IIIb'] + [IIIc']}{[IIa'] + [IIb'] + [IIc'] + [IIIa'] + [IIIb'] + [IIIc'] + [IIa] + [IIb] + [IIc] + [IIIa] + [IIIb] + [IIIc]}. \quad (9)$$

Dang et al. (2016) found that soils with ratios of 6- over 5-methyl brGDGTs that are lower than 0.5, $IR_{6me} < 0.5$, have a higher correlation between MBT' and MAAT. After excluding 173 soils from the global dataset of De Jonge et al. (2014) with $IR_{6me} > 0.5$, Naafs et al. (2017) proposed two new air temperature calibrations with higher R^2 and lower RMSEs than those of De Jonge et al. (2014):

$MAAT_{soil5me} = - 14.5 + 39.09 \times MBT'_{5me}$ (n = 177, R^2 = 0.76, RMSE = 4.1 °C), and (10)

$MAAT_{mrlsoil5me} = 10.0 + 14.7 \times [Ia] – 31.7 \times [IIa]$ (n = 177, R^2 = 0.77, RMSE = 3.8 °C). (11)

These recent calibrations, however, cannot be used to estimate temperatures above 24-25 °C, for when the MBT'_{5me} = 1 in equation 10, the estimated temperature saturates at 24.6 °C. For equation 11, the maximum temperature that this calibration can estimate is 24.7 °C, when the FA of brGDGT-Ia =1 and brGDGT-IIa = 0.

Despite these efforts to improve the global calibration of brGDGT proxies, the scatter in derived temperature estimates remains large (RMSEs ≈ 3.8 – 4.9 °C). Moreover, environmental factors besides temperature may also affect the production of brGDGTs through their source organisms and their distribution in the environment. Precipitation, soil moisture, vegetation cover, bacterial community composition, and growing degree days (GDD) of the source organism above freezing are all known sources of variability in the distribution of brGDGTs in

161 soils (Dang et al., 2016, De Jonge et al., 2019; Menges et al., 2014; Naafs et al., 2017; Peterse et
162 al., 2014, Wang et al., 2014). These environmental factors can vary regionally, and thus affect
163 the sources and distribution of brGDGTs (Ding et al., 2015; Menges et al., 2014; Wang et al.,
164 2016; Yang et al., 2015). Furthermore, the biological source of brGDGTs remains unknown.
165 Acidobacteria were suggested to represent the most likely source of brGDGTs in a soil profile
166 from the Saxnås Mosse peat bog (Weijers et al., 2009). But, only a small number of
167 acidobacteria grown in culturing studies have been shown to produce brGDGTs, and then only a
168 limited number of them (Sinninghe Damsté et al., 2011, 2018). Furthermore, Weber et al. (2018)
169 showed that stratified lake systems can have a redox-dependent differentiation in the bacterial
170 community in water columns with strong redox gradients, which impact the distribution of
171 brGDGTs at different water depths. The biological sources of brGDGTs not only remain largely
172 unknown, but these lipids have also been found in a wide range of environments. Therefore,
173 given the large diversity of bacteria in soils, the few taxa that account for almost half of this
174 diversity, and the role of environmental factors controlling their distribution (Delgado-Baquerizo
175 et al., 2018), it is reasonable to assume that multiple biological sources of brGDGTs are possible
176 in different types of soils.

177 Soil bacteria sense the temperature in the soil, not that of the overlying air. Therefore,
178 scatter in inferences of MAATs may also derive from temperature differences between the soil
179 and air. Finally, ignorance of whether bacteria grow in some, but not all, seasons and in how they
180 sense seasonal variations in temperature adds uncertainty to inferences of temperatures,
181 especially in global datasets spanning different latitudes with differing amplitudes of annual
182 temperature variation (Dearing Crampton-Flood et al., 2020; Deng et al., 2016; Wang et al.,
183 2016; Yang et al., 2014). The tropics provide a modest seasonal cycle, allowing temperature

differences between MAAT and, for example, the warmest month, to be close enough to neglect a possible seasonal uncertainty to infer temperature estimates with these calibrations.

3. Material and methods

3.1 Sampling in the Eastern Cordillera of Colombia

We collected 32 soil samples from 10 and 50 cm depth at 16 sites along two altitudinal transects spanning ~3200 m of elevation, one across the eastern flank (~400 to ~3400 m) and the other across the western flank (~200 to ~2600 m) of the Eastern Cordillera of Colombia (Figure 2). We also collected four more soil samples from a 30 cm depth at four sites on the western flank (218, 1281, 2185, 2589 m) to evaluate variations of brGDGTs with depth. Temperature data loggers (HOBO UA-001-08 8K) were installed at the same depths of 10 and 50 cm where we collected samples for analysis of brGDGTs, and we ensured that the loggers were fully inserted within the wall of the hole at the appropriate depths. We attached a string to each logger and the holes were covered with the same material that was dug out, making sure that the end of the string was left exposed at the surface. Additionally, we installed air-temperature loggers at each site ~2 meters above the ground from the closest tree and at a distance <~15 m from the soil loggers. Soil and air temperature measurements were recorded every two hours from August 2017 to August 2018 (Table S1 in the supporting information). We recovered all loggers, except for the two soil loggers from the lowest (~ 400 m) site on the eastern flank. Soil pH was measured in the field using an Oaktan waterproof pH 150 meter and a WD-35614-30 probe. We mixed ~2 g of soil with milli-Q water in a 1:2.5 (soil:water) ratio before each measurement and used a new container for each sample. We calibrated the pH-meter at every third station using the buffers with pH 4.00, 7.00, and 10.00.

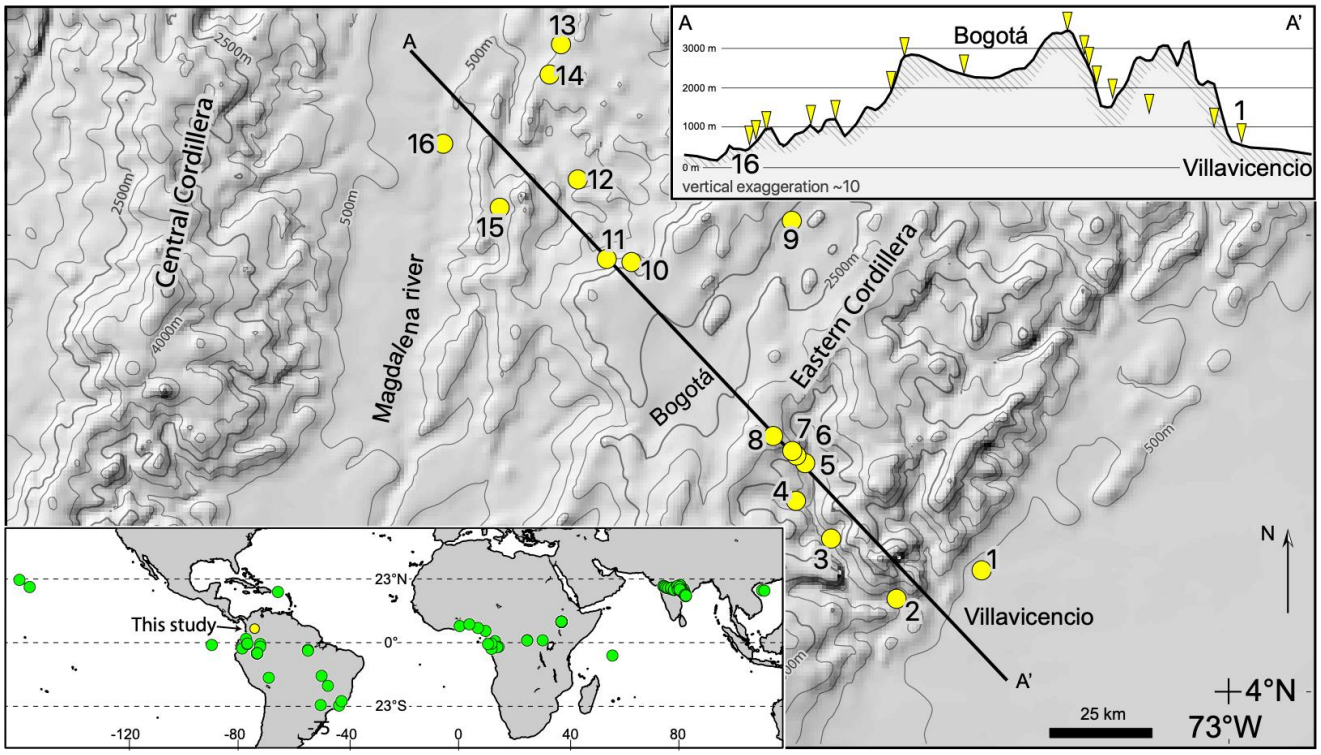

Figure 2. Study area. **a)** Map of the Eastern Cordillera of Colombia for which the regional calibration was generated; yellow symbols indicate the 16 sites with new data presented in this study. The black line indicates the altitudinal transect (from A-A') of the 16 soil sites shown in the insert in the upper right corner. **b)** World map indicating the locations of soils around the tropics used in the tropical compilation.

3.2 brGDGTs analysis of soil samples

We freeze dried, homogenized, and sieved (0.3 mm) the soil samples to remove roots, plant debris, and coarse particles. In order to achieve maximum recovery of lipids from each sample, we extracted ~8 g of soil sample twice with dichloromethane:methanol (DCM:MeOH 9:1 v:v) using an accelerated solvent extractor (ASE 200 DIONEX; 100 °C and 2000 psi). We evaporated total lipid extracts (TLEs) under a gentle N_2 stream using a Turbovap and then combined and removed elemental sulfur using copper pellets previously activated with HCl for at least 1 h. Later, we filtered the TLEs through a short Pasteur pipette filled with glass wool and sand:Na_2SO_4 (8:2) to remove any particles and water. Samples were spiked with 250 ng of the

222 C_{46} GDGT internal standard (Huguet et al., 2006). Then, we dissolved the dry samples in 1ml of
223 hexane:isopropanol (hexane:IPA 99:1 v/v) and sonicated, vortexed, and filtered them through a
224 0.45 μm PTFE filter before injection.

225 We analyzed brGDGTs using a Thermo Scientific Ultimate 3000 high performance liquid
226 chromatograph (HPLC) coupled to a Q Exactive Focus Orbitrap-Quadrupole high resolution
227 mass spectrometer via an atmospheric pressure chemical ionization (APCI) source. We achieved
228 the chromatographic separation, identification, and quantification of brGDGTs by using a slighly
229 modified version of the protocol described by Hopmans et al. (2016). Rather than starting at 18%
230 hexane:isopropanol (9:1, v/v) (Hopmans et al., 2016), we began the eluent gradient with 30%
231 hexane:isopropanol (9:1, v/v) to shorten overall run times without compromising the
232 chromotographic separation of brGDGTs (Crump et al., 2019; Harning et al., 2019). We re-
233 equilibrated the HPLC column for 20 minutes between runs. The injection volume was 10μl
234 instead of the 5μl in Hopmans et al. (2016). The positive ion APCI settings are in Table S2 in the
235 supporting information. We analyzed samples on full-scan mode with a mass range of 500-1500
236 *m/z* at 70,000 mass resolution. We calibrated the Q Exactive within a mass accuracy range of 3
237 ppm using the Pierce LTQ Velos ESI Positive Ion Calibration Solution (Thermo Scientific). We
238 identified brGDGTs based on their characteristic molecular ions and elution patterns and
239 performed manual integration of the area under each peak using the Thermo Scientific Xcalibur
240 software.

241

242 **3.3 Tropical soil dataset compilation**

243 We compiled existing brGDGTs data from sites within 23.5° of the equator from De Jonge et
244 al. (2014), Dearing Crampton-Flood et al. (2020), Jaeschke et al. (2018), and Naafs et al. (2017),

and combined them with the results from our study to create a soil brGDGT calibration that can be used for tropical paleoclimate reconstructions (Table S3 in the supporting information). We included only sites for which 5- and 6-methyl isomers were separated, their fractional abundance (FA) was available, and their modern MAAT was measured. We excluded four soils reported by De Jonge et al. (2014), also excluded by Naafs et al. (2017), because the elevation of those sites was unknown. De Jonge et al. (2014) and Naafs et al. (2017) inferred different values of MAAT, as large as 13 °C for the same site. Naafs et al. (2017) interpolated temperatures from a gridded database with 0.5° of resolution in both latitude and longitude: When the elevation of a soil site fell inside a cell grid but differed by more than 250 m from the average elevation of that grid cell, Naafs et al. (2017) used the temperature value of the nearest grid cell, whose elevation differed from that of site by less than 250 m. We consider that this approach is inappropriate for the tropics, where the biggest temperature differences derive from differences in elevation that can vary across short distances. Therefore, we decided to use the temperatures reported by De Jonge et al. (2014) because they relied on air temperatures from the closest meteorological station.

3.4 Statistical analyses

We chose not to perform simple linear regression using the MBT'$_{5me}$ index, as this index can estimate temperatures only up to 22.7 °C (De Jonge et al., 2014) and 24.6 °C (Naafs et al., 2017). Instead, we carried out multiple linear regressions to derive equations to estimate temperatures, first for the Eastern Cordillera of Colombia and then for the tropics as a whole. The original dataset from De Jonge et al. (2014) excluded all 6-methyl brGDGTs because of their lack of correlation with temperature. We also excluded 5-methyl brGDGTs-IIIb and -IIIc, as they have

been shown to be present in only 26% of global soils (Peterse et al., 2012). We computed the Akaike Information Criterion (AIC, equation 12, Akaike, 1974) for various candidate relationship that relate brGDGTs to MAAT, each with different combinations of predictors. In this case, the predictors were FAs of individual brGDGTs, and the equation with minimum AIC value was selected to be the best fit to the data. The AIC is computed as follows:

$$AIC = -2L + k*\log(n), \qquad (12)$$

where k is the number of parameters estimated by the equation, n is the number of observations, and L is the log-likelihood function. The first term corresponds to the mean squared error (i.e. goodness of fit), and the second term is a penalty for complexity of the equation (i.e. the number of parameters). When comparing two different equations, we used the analysis of variance (ANOVA) to determine whether the difference between their means was statistically significant.

4. Results and Discussion

4.1 Logger temperature data from the Eastern Cordillera of Colombia

Mean monthly air temperatures (MMATs) and mean monthly soil temperatures (MMSTs) recorded by the loggers show a small temperature seasonality in this region, with the greatest difference between the mean warmest month and the mean coldest month for the same site of only 3.27 °C (Figure 3 and Table S1 in the supporting information). Average temperature gradients with elevation across the entire Eastern Cordillera of Colombia are 5.9 °C/km for air ~2 m above the ground, 5.2 °C/km for soil at a 10 cm depth, and 5.3 °C/km for soil at a 50 cm depth (Figure 4). The difference between soil (for both 50 cm and 10 cm) and air temperatures increases with elevation from ~ -0.5 °C to ~2.5 °C (indicating an elevation gradient of the

difference of 0.73 °C/km; Figure 4). Since the mean annual soil temperatures (MASTs) measured at both 10 and 50 cm at each station of the Eastern Cordillera of Colombia were almost identical, with an average absolute difference of 0.1 °C (Figure 4), we included temperatures from both depths in the following calibration.

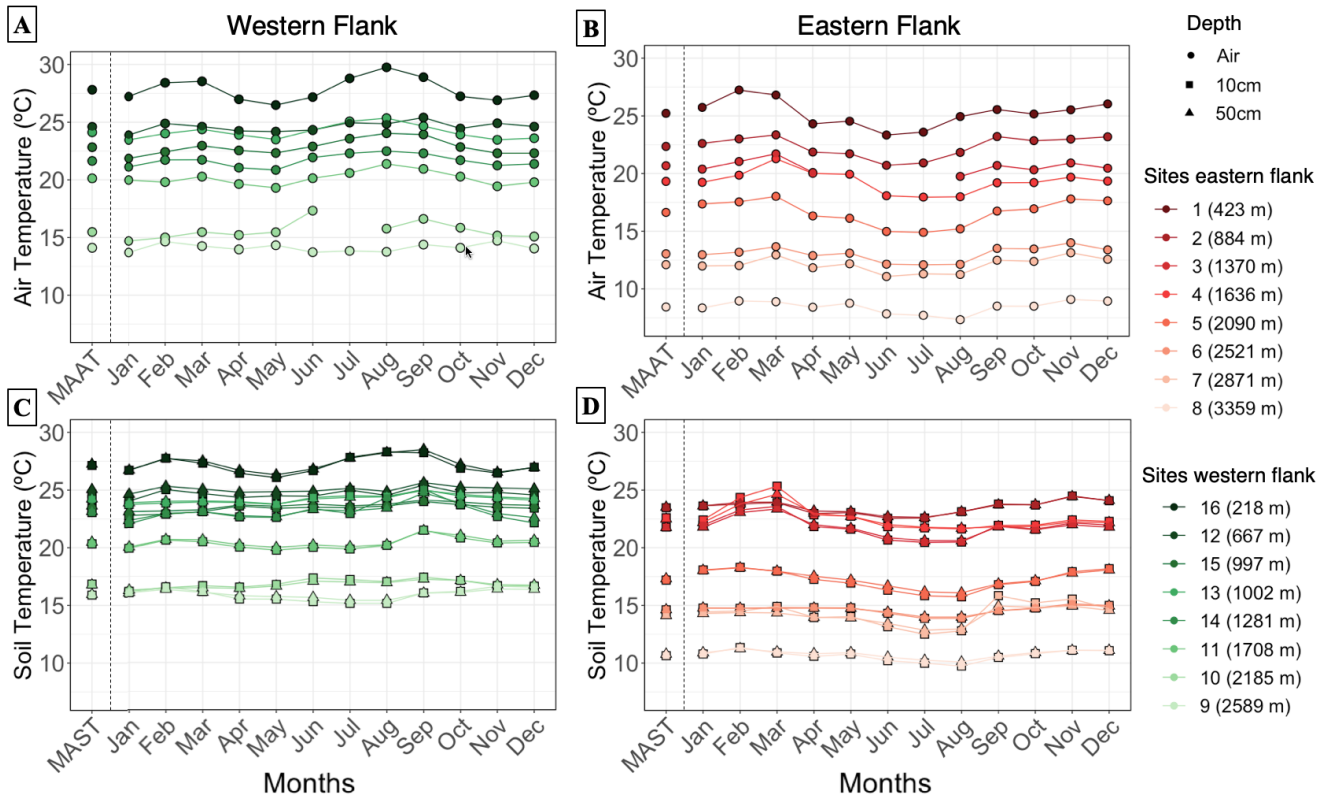

Figure 3. Mean monthly temperatures recorded by data loggers from August 2017 to August 2018 along the two elevation transects in the Eastern Cordillera of Colombia. Panels **(a)** and **(b)** show the Mean Monthly Air Temperature (MMAT) for each flank. Panels **(c)** and **(d)** show the Mean Monthly Soil Temperature (MMST) at 10 and 50 cm depths for each flank. Each plot shows the mean annual air temperature (MAAT) and mean annual soil temperature (MAST) for each site on the left-hand side adjacent to the y-axis.

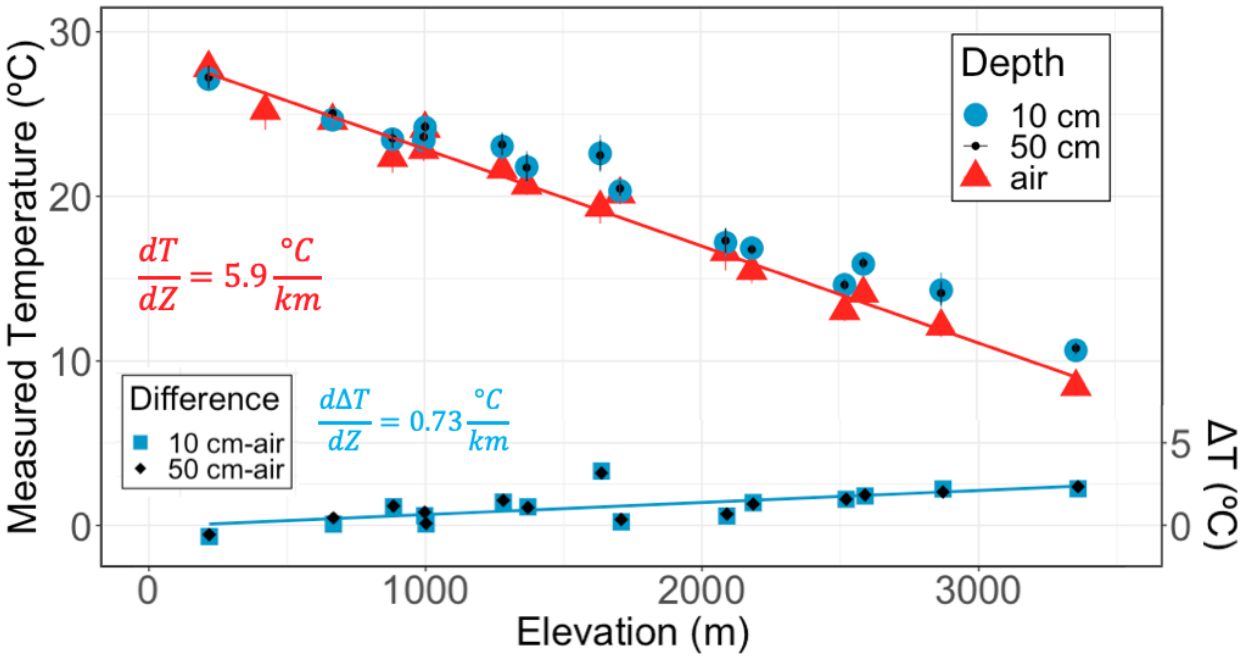

Figure 4. Mean *in situ* soil and air temperatures measured from August 2017 to August 2018 versus elevation. Top: points show mean temperatures at 10cm (blue circles) and 50cm (black circles), and overlying air temperatures (red triangles), with their respective monthly standard deviations. The red line shows a gradient of air temperature relative to elevation in the Eastern Cordillera of 5.9ºC/km. Bottom: points show differences between mean temperatures of soil (at 10 cm: blue squares and at 50 black diamonds) and air. The blue line shows a gradient of the difference in temperature relative to elevation of 0.73°C/km.

4.2 Regional soil brGDGTs calibration for the Eastern Cordillera of Colombia

We compare the new measured soil brGDGTs data from the Eastern Cordillera of Colombia with the measured pH and MAAT (Table S3 in the supporting information) in Figures 5 and 6, respectively. Figure 5 shows regressions between the fractional abundance (FA) of each individual brGDGT with pH. Most 6-methyl brGDGTs (those in columns II' and III' of Figure 5) show a higher correlation with pH than 5-methyl brGDGTs (those in columns II and III of Figure 5). The highest correlation with pH comes from the brGDGT-IIb' (R^2 = 0.57). Consistent with previous work (De Jonge et al., 2014), 6-methyl brGDGTs correlate better with pH than with

MAAT, demonstrating that these isomers are not needed for the establishment of a temperature calibration and therefore can be excluded from it.

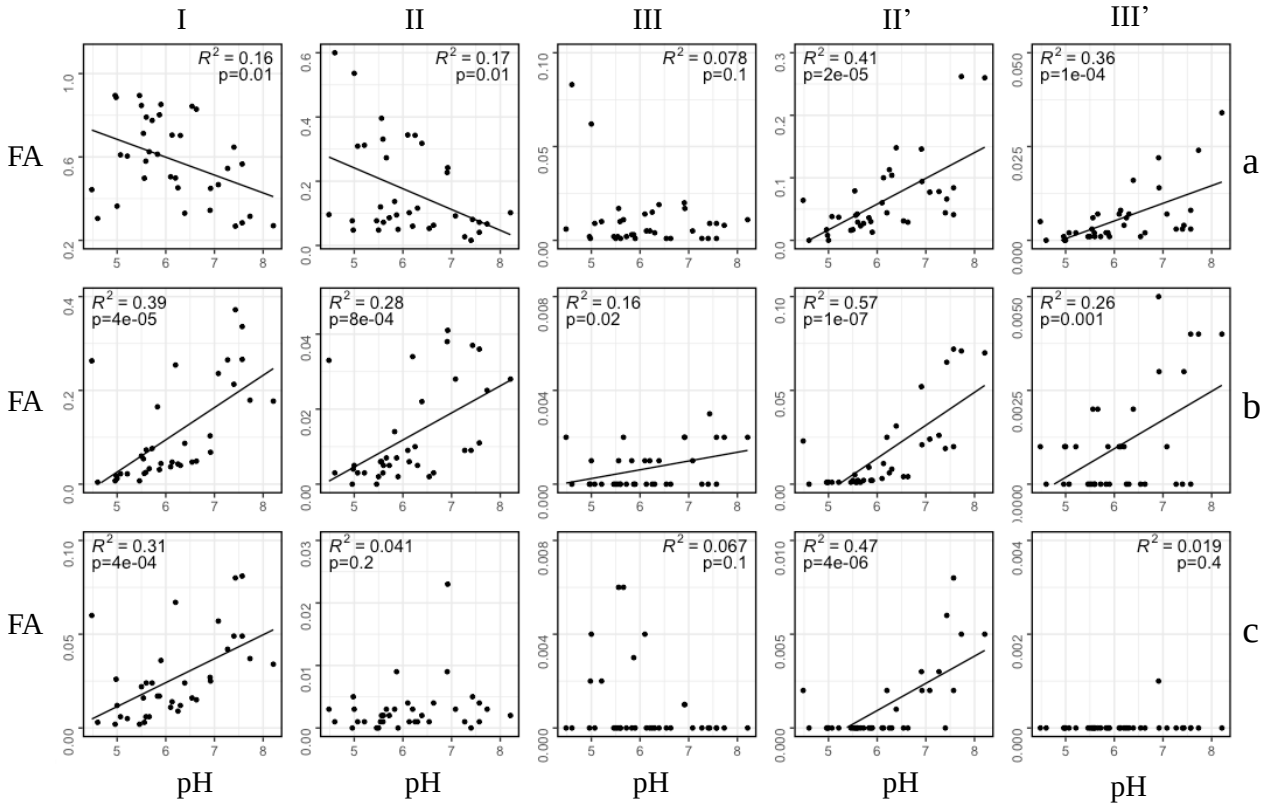

Figure 5. Regressions between fractional abundances (FA) of brGDGTs and measured soil pH from the Eastern Cordillera of Colombia. Roman numerals and letters on the right refer to the different brGDGT structures, II' and III' correspond to the structures with C6-methylation position. Linear regressions are shown for those brGDGTs with an $R^2 \geq 0.1$, with the corresponding values of *p*.

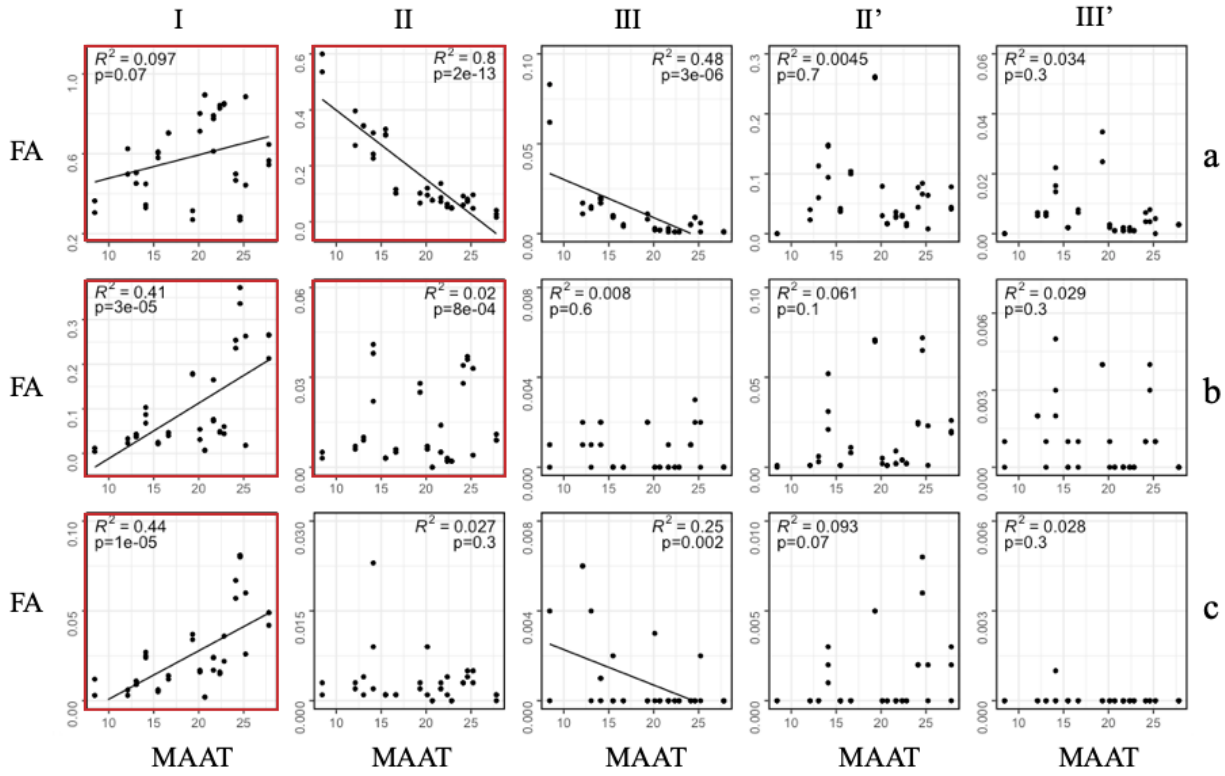

Figure 6. Regressions between fractional abundances (FA) of brGDGTs and measured mean annual air temperatures (MAAT) of each soil in the Eastern Cordillera of Colombia. Roman numerals and letters on the right refer to the different brGDGT structures, II and III correspond to the structures with C5-methylation position. Linear regressions are shown for those brGDGTs with $R^2 \geq 0.1$, with the corresponding values of *p*. Red boxes show the brGDGTs used in the regional air calibration (equation 14).

Putting together the modern soil brGDGTs data presented in Figure 6 and the MAAT and MAST derived from loggers (Figure 3), we developed air and soil temperature calibrations for the Eastern Cordillera of Colombia. Although we obtained similar AIC values (21.25 and 21.65) from the two best equations for the soil temperature calibration, we selected the one with the second lowest AIC value (equation 13):

$$\text{MAST} = 18.79 + 4.07 \times [\text{Ia}] + 28.73 \times [\text{Ib}] - 17.3 \times [\text{IIa}] - 81.22 \times [\text{IIb}] \quad (13)$$

(n = 30, R^2 = 0.93, RMSE = 1.2 °C),

The selected equation includes brGDGT-Ia, which is a common and abundant brGDGT in warm environments. The two equations show no statistically significant difference in the variances captured. It is not uncommon to have equations with AIC values close to each other around the minimum value. Although a single best equation is identified, it is good to consider other close equations, such as the case here (e.g., Mendoza et al., 2014; Regonda et al., 2006, and references therein).

For the air temperature calibration, equation 14 yields the smallest AIC value:

$$MAAT = 10.93 + 11.29 \times [Ia] + 32.39 \times [Ib] + 53.22 \times [Ic] - 11.84 \times [IIa] - 79.94 \times [IIb] \quad (14)$$

($n = 36$, $R^2 = 0.95$, RMSE = 1.1 °C).

Both regional MAAT and MAST calibrations reduce the RMSE substantially, from 4.6 °C (equation 8, De Jonge et al., 2014) and 3.8 °C (equation 11, Naafs et al., 2017), to 1.1 °C for MAAT and 1.2 °C for MAST (Figure 7a, b, d, e). Moreover, all air and soil temperatures implied by the regional calibrations differ from those measured with temperature loggers by less than 5 °C (Figure 8). By contrast, global calibrations underestimate air temperatures for the Eastern Cordillera of Colombia by up to 13.2 °C. Equations 13 and 14 provide a more precise reconstruction of temperatures in this region than the global calibrations (Figure 7). These regional calibrations not only allow for a larger range of temperature reconstruction than previous global calibrations (De Jonge et al., 2014: Naafs et al., 2017; Peterse et al., 2012), but also extend the temperature measurements within the calibration to higher values (27.8 °C for air and 27.5 °C for soil). MAAT and MAST estimates outside these calibration ranges, however, should be made with caution, as they rely on extrapolations.

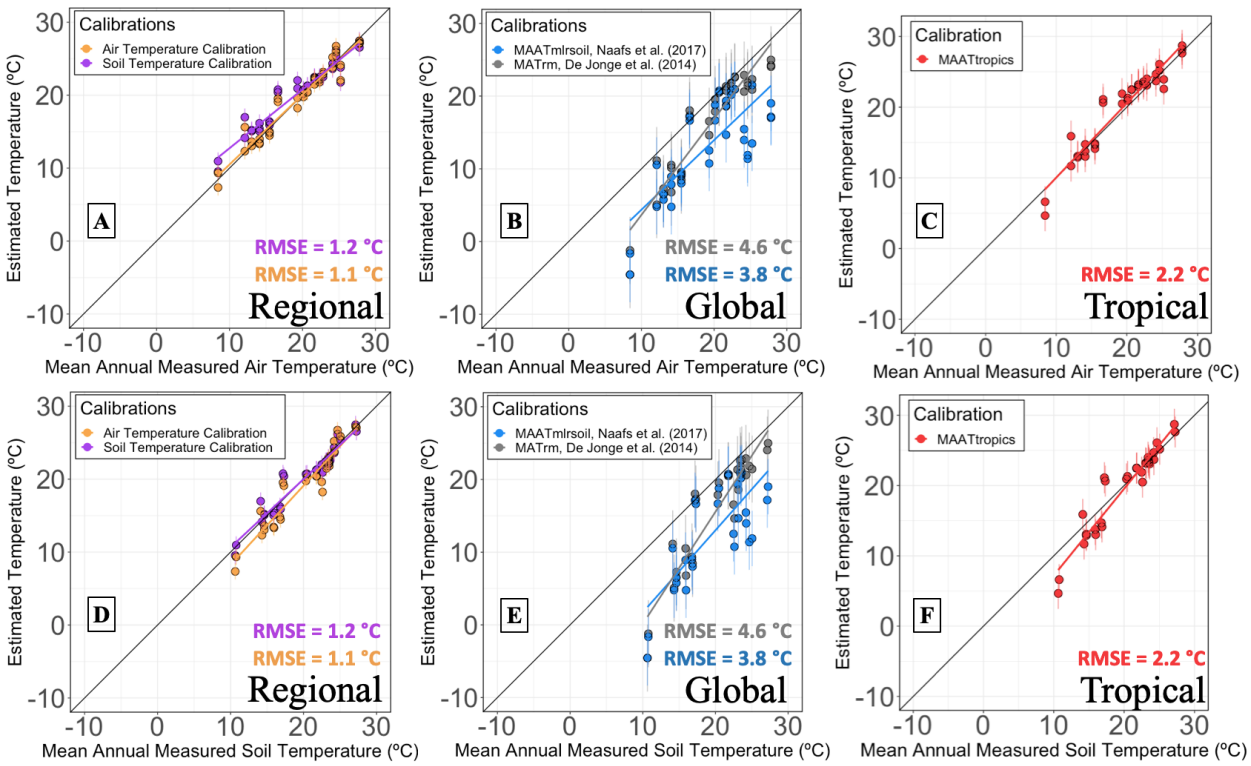

Figure 7. Regressions of estimated temperatures against measured Mean Annual Air Temperatures (a, b, and c) and Mean Annual Soil Temperatures (d, e, f) from August 2017 to August 2018 in the Eastern Cordillera, using temperatures estimated with different brGDGT calibrations. In figures **a** and **d**, temperatures inferred from brGDGTs are compared using the regional calibrations for air temperatures (orange) (equation 14) and soil temperatures (purple) (equation 13). In figures **b** and **e**, temperature values are compared with global calibrations (equations 8 and 11) from De Jonge et al. (2014) (gray) and Naafs et al. (2017) (light blue). In panels **c** and **f**, temperature values are compared with the tropical calibration (equation 16). Black lines represent 1:1 relationships.

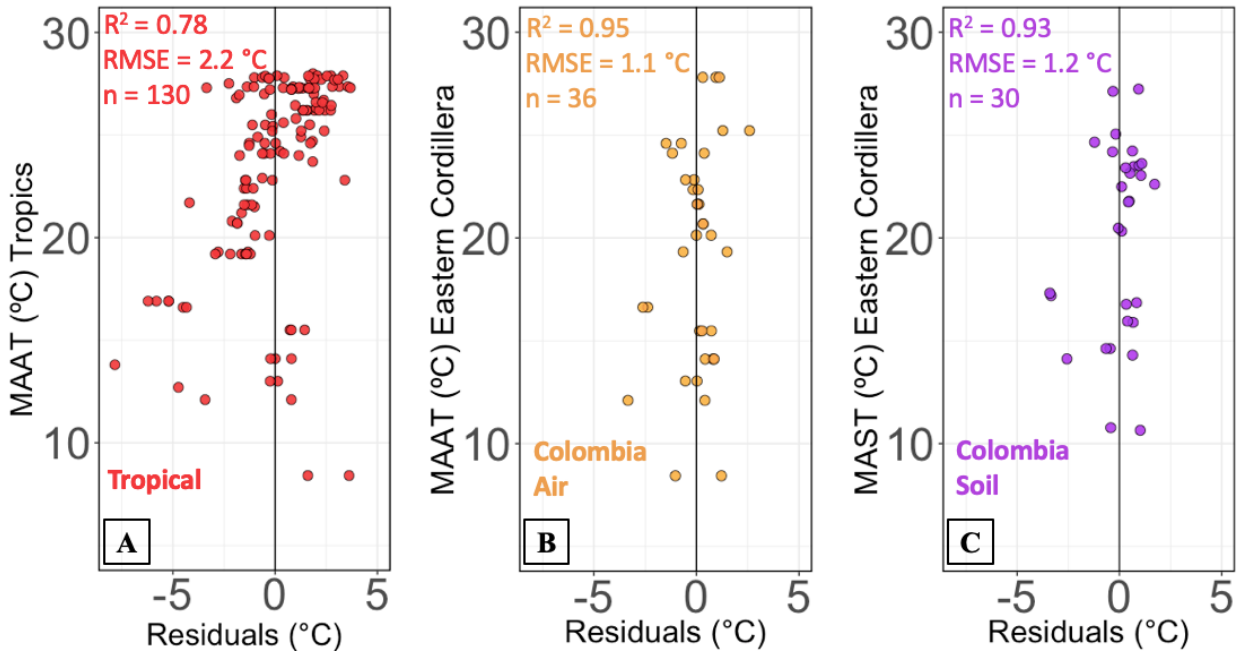

Figure 8. Residuals for the three multiple linear regressions calculated in this study. **(a)** the MAAT tropical calibration, **(b)** the air temperature calibration of the Eastern Cordillera of Colombia, and **(c)** the soil temperature calibration of the Eastern Cordillera of Colombia.

Previous work on the Eastern Cordillera of Colombia by Anderson et al. (2014), which used a chromatographic method that did not separate 5- and 6- methyl brGDGTs, yielded a local soil calibration with an RMSE of 2.9 °C (equation 15):

$$\text{MASTsoil} = 29.1 - 0.017 \times (\text{Ia}) - 0.61 \times \log(\text{Ib}) - 3.34 \times \log(\text{Ic}) - 0.34 \times (\text{IIa+IIa'}) - 0.11 \times \log(\text{IIb + IIb'}) + 0.44 \times \log(\text{IIc + IIc'}) - 0.067 \times (\text{IIIa + IIIa'}) \quad (15)$$

(n = 24, R^2 = 0.77, RMSE = 2.9 °C),

Although this equation resulted in an improvement over the RMSE of 5 °C from the global air temperature calibration (equation 5, Peterse et al., 2012), this value is still higher than what can be obtained when 6-methyl brGDGTs are chromatographically separated and excluded (equation 13, Figure 9). The influence of 6-methyl brGDGTs is particularly noticeable at the warm sites (>15 °C), where the calibration from Anderson et al. (2014) underestimates temperatures by as

much as ~9 °C. Furthermore, for sites where we measured MAST, we obtained an R^2 = 0.93 with the soil calibration in equation 13 compared to the R^2 = 0.52 for the calibration of Anderson et al. (2014). This improvement confirms the utility of separating 5- and 6-methyl brGDGTs when estimating temperatures.

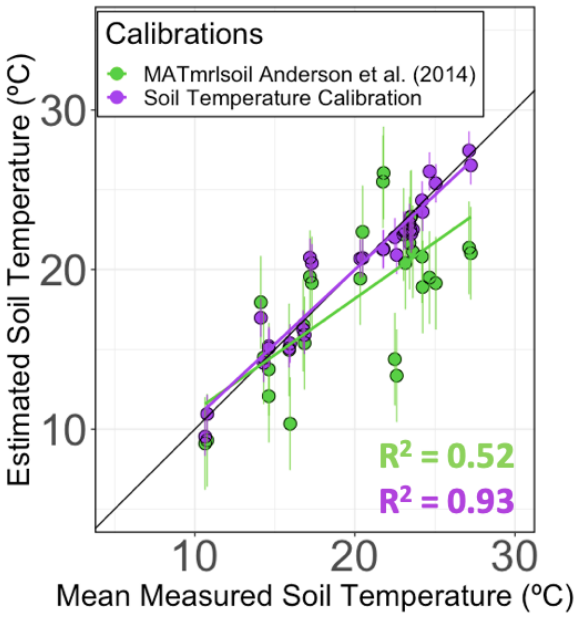

Figure 9. Comparison between the soil calibration from Anderson et al. (2014) (green, equation 15) and the regional soil calibration (purple, equation 13) with soil temperature measurements from the Eastern Cordillera of Colombia.

4.3 Integrating brGDGTs for a pan-tropical soil calibration

In order to integrate the new data obtained from the Eastern Cordillera of Colombia into datasets from elsewhere in the tropics, we compared the available measured pH and MAAT for each soil in the tropical compilation (Table S3 in the supporting information) with the FA of each individual brGDGT (Figures 10 and 11, respectively). From all soil data available, the regressions in Figures 10 and 11 only include 83 samples, as Dearing Crampton-Flood et al. (2020) reported only two decimal values for the FA of each brGDGTs and no pH measurement.

403 The 6-pentamethyl brGDGTs exhibit the highest correlation with pH in the 83 soil samples from
404 the tropical compilation (Figure 10), as reported for our data (Figure 5) and as previously
405 suggested by De Jonge et al. (2014). These isomers also exhibit an insignificant correlation with
406 MAAT (e.g., R^2 = 0.12; *p*-value = 0.002 for IIa', Figure 11). Furthermore, only 2 out of 130 soil
407 samples from this tropical compilation have a FA higher than 0.006 for 5-methyl brGDGT-IIIb
408 and -IIIc (Figure 11). Since these samples represent only 1.5% of the tropical dataset, we
409 excluded brGDGT-IIIb and brGDGT-IIIc from temperature calibrations.

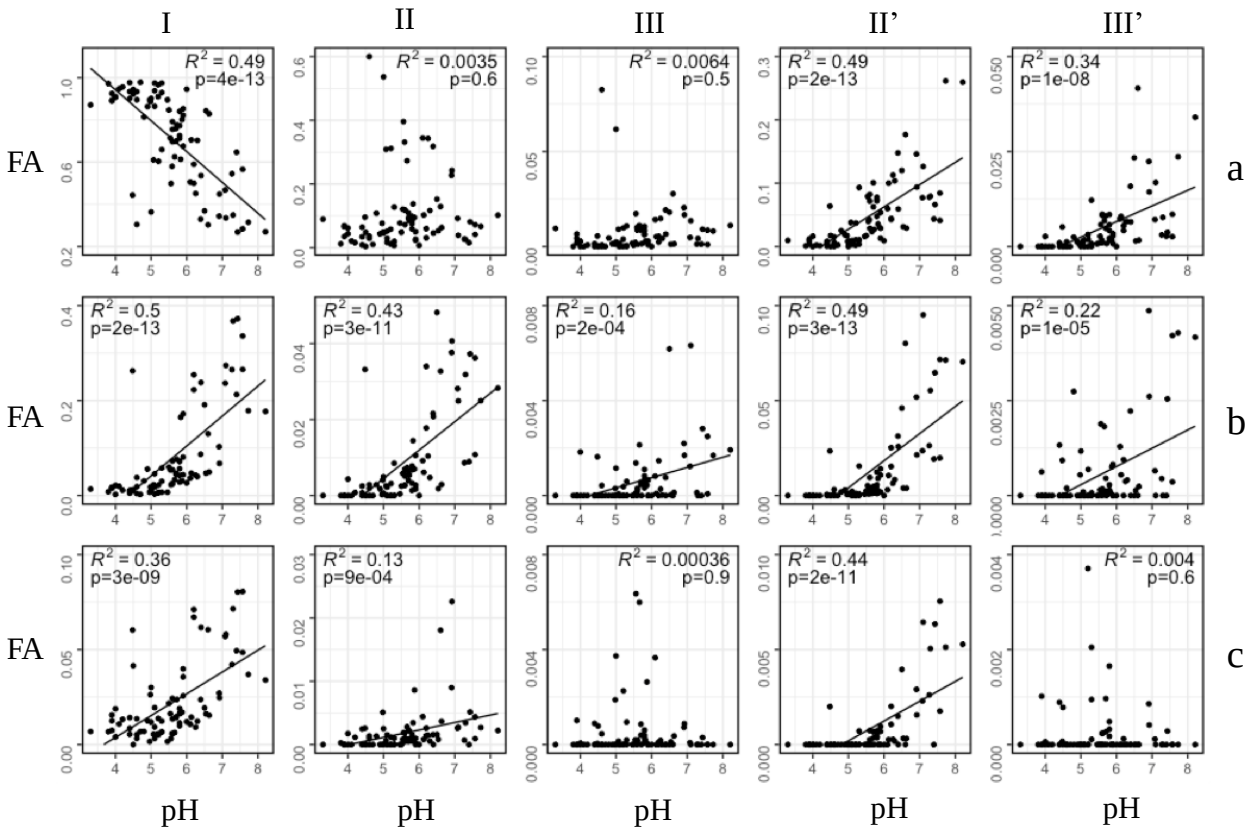

Figure 10. Regressions between fractional abundances (FA) of brGDGTs and measured soil pH from the compilation of brGDGT measurements from the tropics. Only 83 out of 130 soil samples have reported pH measurements. Roman numerals and letters on the right refer to the different brGDGT structures, II' and III' correspond to the structures with C6-methylation position. Linear regressions are shown for those brGDGTs with an $R^2 \geq 0.1$, with the corresponding values of *p*.

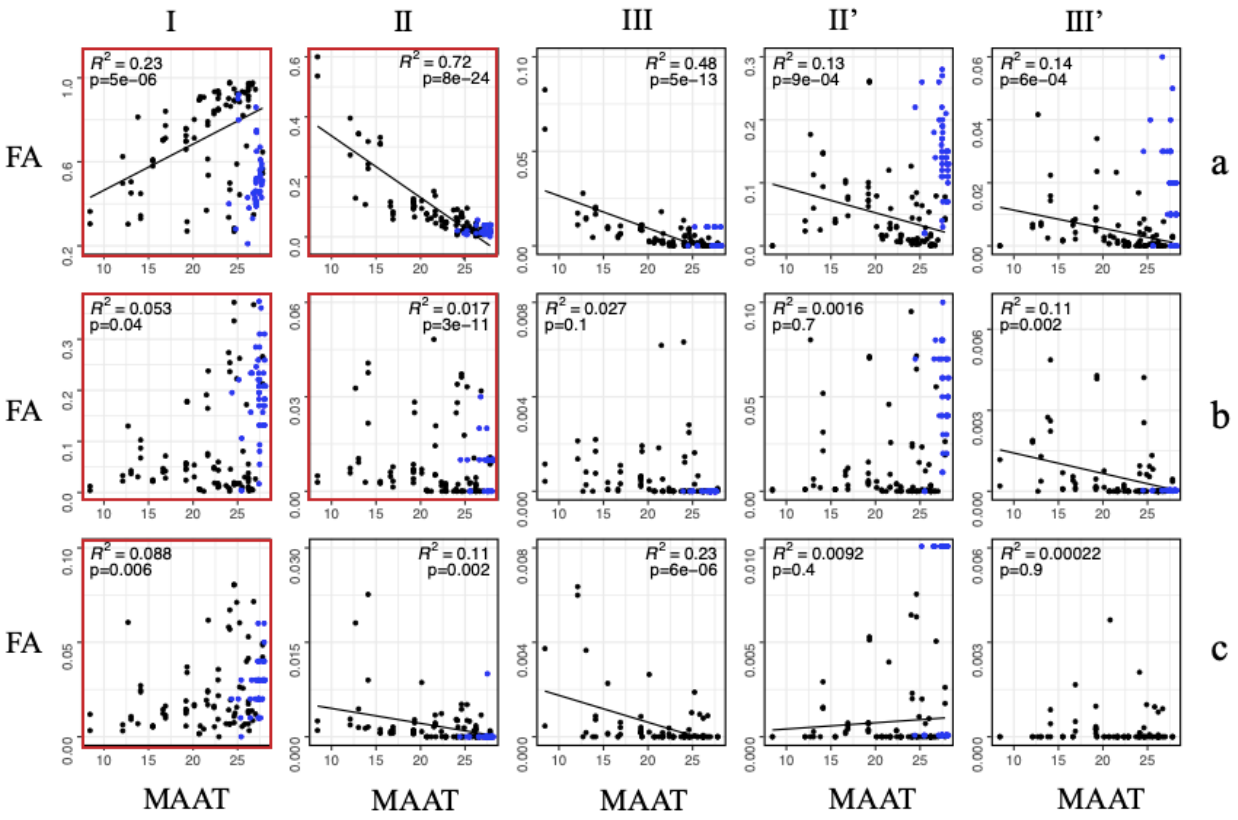

Figure 11. Regressions between fractional abundances (FA) of brGDGTs and measured mean annual air temperatures (MAAT) of each soil in the tropical compilation. Roman numerals and letters on the right refer to the different brGDGT structures, II' and III' correspond to the structures with C6-methylation position. Linear regressions are shown for those brGDGTs with $R^2 \geq 0.1$, with the corresponding values of *p*, and are done only with 83 soil samples. Data reported from India (Dearing Crampton-Flood et al., 2020) are shown in blue but were not used in the linear regressions for each brGDGT. Red boxes show brGDGTs used in the tropical calibration (equation 16).

brGDGT-IIa has the highest correlation with MAAT (R^2 = 0.71 in 83 soil samples; Figure 11). In general, brGDGT-Ia has the highest FA in warm and tropical regions, but our results suggest that variations in temperature in these regions are better captured by brGDGT-IIa. Both of these brGDGTs, along with brGDGT-Ib, -Ic, and -IIb, correlate best with temperature in tropical areas where the seasonal cycle of temperature is small. When all tropical data are used, equation 16 fits data best, according to the AIC criterion:

$$MAAT_{tropics} = 17.55 + 7.45 \times [Ia] + 36.16 \times [Ib] - 28.89 \times [Ic] - 25.02 \times [IIa] - 69.22 \times [IIb] \quad (16)$$

(n = 130, R^2 = 0.78, RMSE = 2.2 °C).

Although equation 16 exhibits a larger RMSE (2.2 °C) than the regional air temperature calibration (1.1 °C, equation 14), it is roughly half that of global calibrations (RMSE = 3.8-4.6 °C; Figure 7).

Global calibrations (equation 8, De Jonge et al., 2014; equation 11, Naafs et al., 2017) underestimate temperature in tropical sites by as much as ~ -16 °C. The global calibration by De Jonge et al. (2014) has the same R^2, 0.78, as our tropical calibration, but the RMSE of the tropical calibration is less than half (2.2 °C) that of the global calibration (4.6 °C). When considering sites with lower temperatures, which come from higher sites in the case of the tropics, the tropical calibration slightly overestimates the temperatures at these sites (Figure 12). A possible explanation for this overestimation is the limited number of sites (11 out of 130) with a MAAT below 15 °C in the tropical compilation, which may lead to biases towards warmer estimates. Another possible contribution to this underestimation could be the observed increasing difference between soil and air temperatures with increasing elevation (Figure 4), where bacteria living in high-elevation soils (>3000 m) register the warmer temperature of the soil compared to the colder overlying air.

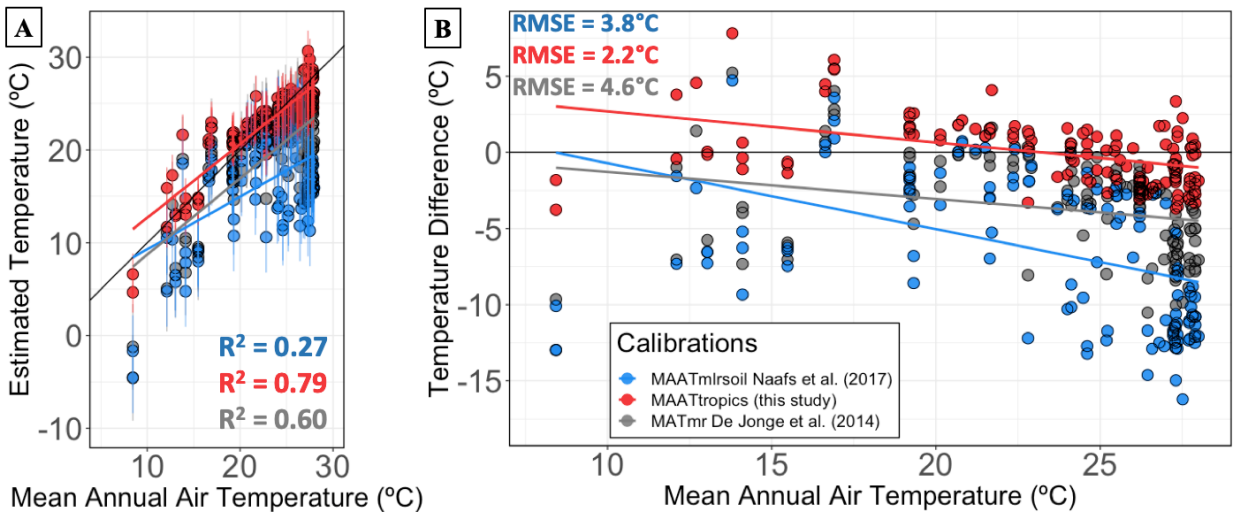

Figure 12. **a)** Comparison between tropical (equation 16) and global (equations 8 and 11) calibrations for air temperatures using all tropical sites. **b)** Differences between the estimated and the measured temperatures for each tropical soil versus measured MAAT (n = 130).

Global calibrations of MAAT rely on soil bacteria that live at different latitudes and that can grow at different times within a year. Whether bacteria that live in the soil grow all year round, or solely on the days above freezing, or during a specific season is still unknown. Therefore, temperature estimates that are calibrated with global MAAT could misrepresent the temperatures that bacteria record. If bacterial growth were biased towards warmer than colder days, global calibrations would underestimate temperature. In order to quantify the typical temperature variability in an annual cycle at different latitudes, we obtained terrestrial air temperature data from around the world for the 2000-2018 period from the European Centre for Medium Range Weather Forecasts (ECMWF) Reanalysis version 5 (ERA5) with a resolution of 0.25° in both latitude and longitude (Hersbach et al., 2019). Figure 13a shows the average MAAT (green), mean warmest month (red), and mean coldest month (blue) of terrestrial temperatures. Figure 13b shows the mean annual range of temperature by latitude, calculated as the difference between the warmest month and the coldest month for terrestrial temperatures. The tropics are

466 the only place where all of regressions of brGDGTs abundances against MAAT, mean annual
467 temperature above freezing, and warmest months are similar enough that they can all represent
468 the same value. Thus, lipid-based proxy calibrations might be better constrained by regional
469 calibrations limited to restricted latitudinal ranges rather than global generalizations.
470

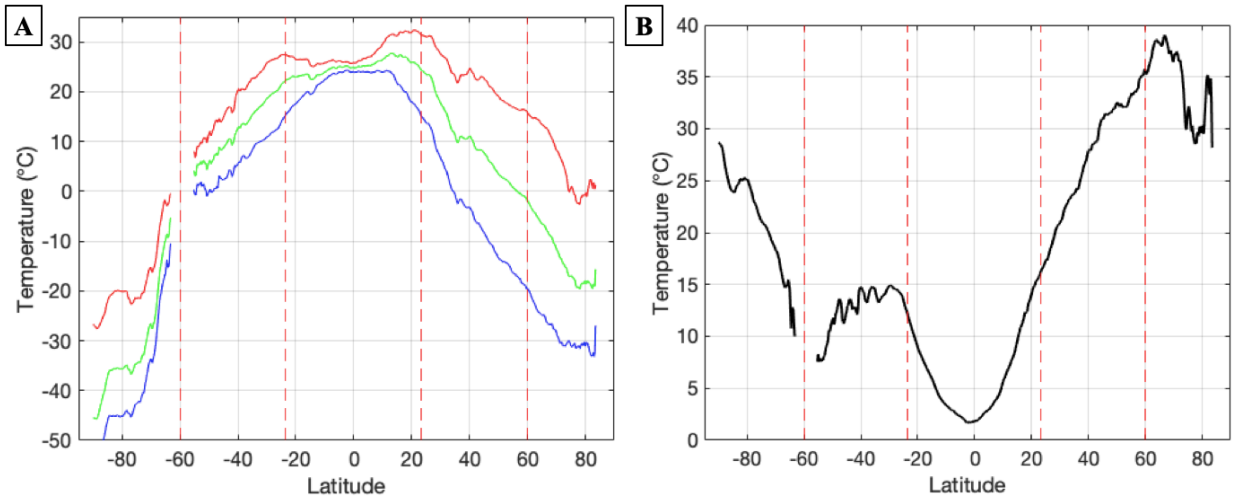

471

472 **Figure 13. a)** Zonally averaged mean air temperatures at 2 m above land areas (obtained from climate
473 copernicus ERA5 data). Mean annual air temperature (green), mean warmest month (red), and mean
474 coldest month (blue). **b)** Zonally averaged mean annual range of air temperature calculated as the
475 difference between the warmest month and the coldest month for each site.
476

477 ## 5. Conclusions

478 We measured temperatures in soils at depths of 10 cm and 50 cm, and in the air 2 m above
479 the ground along profiles spanning 3200 m on the eastern and western sides of the Eastern
480 Cordillera of Colombia. We also took soil samples from the same depths and measured the
481 fractional abundances of the different brGDGTs in them with the goal of improving calibrations
482 of temperatures inferred from brGDGTs to *in situ* temperatures. We obtained linear equations 13
483 and 14 relating the fractional abundances of certain brGDGTs to soil and overlying air

484 temperatures with RMSE of 1.2 °C and 1.1 °C, respectively. Combining these data with
485 published measurements from other sites in the tropics, with latitudes < 23.5°, we obtained a
486 calibration of air temperature (equation 16) with an RMSE of 2.2 °C for use in other tropical
487 locations. These calibrations contrast with, and improve upon, global calibrations with RSME or
488 3.8 – 4.9 °C. Tropical calibrations are not subjected to possible seasonal biases as mean monthly
489 temperatures differ little from the mean annual values. Moreover, these calibrations extend the
490 temperature range accessible by brGDGTs to temperatures typical of low-latitudes, which is
491 necessary for brGDGTs to be used to infer past temperatures from tropical environments,
492 especially during intervals of greenhouse conditions, such as the Early Pliocene, Eocene, and
493 Cretaceous.

Acknowledgements

This research was supported by the Fondo Corrigan-ACGGP-ARES (Colombia), a Lewis and Clark grant, CIRE's Innovative Research Program (IRP) 2017, a CIRES Graduate Student Research Award, a Figueroa Family Grant from the Graduate School at University of Colorado Boulder, an Edward Fellowship from the Department of Geological Sciences at the University of Colorado Boulder, the DIDI (Dirección de Investigación, Desarrollo e Innovación) from Universidad del Norte, the Facultad de Ciencias from Universidad de Los Andes, and NSF grant 1929199. J.S. acknowledges laboratory and analytical support provided by the University of Colorado Boulder. L.P.A. thanks K. Karnauskas for his help with the ERA5 data acquisition and MATLAB coding, and J. Yarce for his help with MATLAB. We thank K. Quinn, N. Kentwortz, K. Amara, and J. Smith for laboratory support, C.A. Rosero, R. Villamil, M.E. Angel-Olaya, E. Pérez-Angel, and F. Gutierrez for assistance in the field, and local residents in Colombia who helped us and allowed us to install temperature loggers on their properties. The data used are listed under Data Availability Statement and cited in the references.

Data Availability Statement

Soil dataset is currently being archived in the Pangaea data repository and will be made available at acceptance.

Global climate data used in this study are freely and publicly available online, and may be accessed directly as:

ECMWF Reanalysis version 5:

https://cds.climate.copernicus.eu/#!/search?text=ERA5&type=dataset

References

Akaike, H. (1974). A new look at the statistical model identification. IEEE Transactions on Automatic Control, 19 (6): 716–723, doi:10.1109/TAC.1974.1100705, MR 0423716.

Anderson, V. J., T. M. Shanahan, J. E. Saylor, B. K. Horton, and A. R. Mora. (2014), Sources of local and regional variability in the MBT'/CBT paleotemperature proxy: Insights from a modern elevation transect across the Eastern Cordillera of Colombia, *Organic Geochemistry*, *69*, 42–51.

Crump, S. E., Miller, G. H., Power, M., Sepúlveda, J., Dildar, N., Coghlan, M., & Bunce, M. (2019). Arctic shrub colonization lagged peak postglacial warmth: Molecular evidence in lake sediment from Arctic Canada. Global change biology, 25(12), 4244-4256.

Dang, X., Yang, H., Naafs, B. D. A., Pancost, R. D., & Xie, S. (2016). Evidence of moisture control on the methylation of branched glycerol dialkyl glycerol tetraethers in semi-arid and arid soils. Geochimica et Cosmochimica Acta, 189, 24–36. https://doi.org/10.1016/j.gca.2016.06.004

De Jonge, C., Hopmans, E. C., Zell, C. I., Kim, J. H., Schouten, S., & Damsté, J. S. S. (2014). Occurrence and abundance of 6-methyl branched glycerol dialkyl glycerol tetraethers in soils: Implications for palaeoclimate reconstruction. Geochimica et Cosmochimica Acta, 141, 97-112.

De Jonge, C., Radujković, D., Sigurdsson, B. D., Weedon, J. T., Janssens, I., & Peterse, F. (2019). Lipid biomarker temperature proxy responds to abrupt shift in the bacterial community composition in geothermally heated soils. Organic Geochemistry, 137, 103897.

Dearing Crampton-Flood, E., Tierney, J. E., Peterse, F., Kirkels, F. M., & Damsté, J. S. S. (2020). BayMBT: A Bayesian calibration model for branched glycerol dialkyl glycerol tetraethers in soils and peats. Geochimica et Cosmochimica Acta, 268, 142-159.

Dekens, P. S., Ravelo, A. C., & McCarthy, M. D. (2007). Warm upwelling regions in the Pliocene warm period. Paleoceanography, 22(3).

Delgado-Baquerizo, M., Oliverio, A. M., Brewer, T. E., Benavent-González, A., Eldridge, D. J., Bardgett, R. D., Maestre, F.T., Singh, B.K., & Fierer, N. (2018). A global atlas of the dominant bacteria found in soil. Science, 359(6373), 320-325.

Deng, L., Jia, G., Jin, C., & Li, S. (2016). Warm season bias of branched GDGT temperature estimates causes underestimation of altitudinal lapse rate. Organic geochemistry, 96, 11-17.

Ding, S., Xu, Y., Wang, Y., He, Y., Hou, J., Chen, L., & He, J. S. (2015). Distribution of branched glycerol dialkyl glycerol tetraethers in surface soils of the Qinghai-Tibetan Plateau: Implications of brGDGTs-based proxies in cold and dry regions. Biogeosciences, 12(11), 3141–3151. https://doi.org/10.5194/bg-12-3141-2015

Ghosh, P., Adkins, J., Affek, H., Balta, B., Guo, W., Schauble, E. A., Schrag, D., & Eiler, J. M. (2006). 13C–18O bonds in carbonate minerals: a new kind of paleothermometer. Geochimica et Cosmochimica Acta, 70(6), 1439-1456.

Groeneveld, J., Steph, S., Tiedemann, R., Garbe-Schönberg, C., Nürnberg, D., & Sturm, A. (2006). Pliocene mixed-layer oceanography for Site 1241, using combined Mg/Ca and δ 18 O analyses of Globigerinoides sacculifer. In Proceedings of the Ocean Drilling Program: Scientific Results (Vol. 202, pp. 1-27).

Hanna, A. J., Shanahan, T. M., & Allison, M. A. (2016). Distribution of branched GDGTs in surface sediments from the Colville River, Alaska: Implications for the MBT′/CBT paleothermometer in Arctic marine sediments. Journal of Geophysical Research: Biogeosciences, 121(7), 1762-1780.

Harning, D.J., Andrews, J.T., Belt, S.T., Cabedo-Sanz, P., Geirsdóttir, Á., Dildar, N., Miller, G.H. and Sepúlveda, J., 2019. Sea ice control on winter subsurface temperatures of the North Iceland Shelf during the Little Ice Age: A TEX86 calibration case study. Paleoceanography and Paleoclimatology.

Herbert, T. D., Peterson, L. C., Lawrence, K. T., & Liu, Z. (2010). Tropical Ocean Temperatures Over the, 328 (June), 1530–1535. https://doi.org/10.1126/science.1185435

Herbert, T. D., Lawrence, K. T., Tzanova, A., Peterson, L. C., Caballero-Gill, R., & Kelly, C. S. (2016). Late Miocene global cooling and the rise of modern ecosystems. Nature Geoscience, 9(11), 843-847.

Hersbach, H., Bell, W., Berrisford, P., Horányi, A., Sabater, J. M., Nicolas, J., Radu, R., Schepers, D., Simmons, A., Soci, C., & Dee, R. (2019), Global reanalysis: goodbye ERA-Interim, hello ERA5. ECMWF Newsletter, 159, 17-24. doi: 10.21957/vf291hehd7

Hooghiemstra, H., Wijninga, V. M., & Cleef, A. M. (2006). The paleobotanical record of Colombia: Implications for biogeography and biodiversity. Annals of the Missouri Botanical Garden, 93(2), 297–325. https://doi.org/10.3417/0026-6493(2006)93%5B297:TPROCI%5D2.0. CO;2

Hopmans, E. C., Schouten, S., & Sinninghe Damsté, J. S. (2016). The effect of improved chromatography on GDGT-based palaeoproxies. Organic Geochemistry, 93, 1–6. https://doi.org/10.1016/j.orggeochem.2015.12.006

Huguet C., Hopmans E. C., Febo-Ayala W., Thompson D. H., Sinninghe Damsté, J. S. and Schouten S. (2006) An improved method to determine the absolute abundance of glycerol dibiphytanyl glycerol tetraether lipids. Org. Geochem. 37, 1036–1041

Jaeschke, A., Rethemeyer, J., Lappé, M., Schouten, S., Boeckx, P., & Schefuß, E. (2018). Influence of land use on distribution of soil n-alkane δD and brGDGTs along an altitudinal transect in Ethiopia: Implications for (paleo)environmental studies. Organic Geochemistry, 124, 77–87. https://doi.org/10.1016/j.orggeochem.2018.06.006

Lawrence, K. T., Liu, Z., & Herbert, T. D. (2006). Evolution of the eastern tropical Pacific through Plio-Pleistocene glaciation. Science, 312(5770), 79-83.

Liu, X.-L., Leider, A., Gillespie, A., Gröger, J., Versteegh, G.J.M., Hinrichs, K.-U. (2010). Identification of polar lipid precursors of the ubiquitous branched GDGT orphan lipids in a peat bog in Northern Germany. Organic Geochemistry 41, 653–660. doi:10.1016/j.orggeochem.2010.04.004

Liu, X.-L., Summons, R.E., Hinrichs, K.-U. (2012). Extending the known range of glycerol ether lipids in the environment: structural assignments based on tandem mass spectral fragmentation patterns. Rapid Communications in Mass Spectrometry 26, 2295–2302. doi:10.1002/rcm.6355

Liu, X.-L., Zhu, C., Wakeham, S.G., Hinrichs, K.-U. (2014). In situ production of branched glycerol dialkyl glycerol tetraethers in anoxic marine water columns. Marine Chemistry 166, 1–8. doi:10.1016/j.marchem.2014.08.008

Lu, H., Liu, W., Wang, H., & Wang, Z. (2016). Variation in 6-methyl branched glycerol dialkyl glycerol tetraethers in Lantian loess–paleosol sequence and effect on paleotemperature reconstruction. Organic Geochemistry, 100, 10–17. https://doi.org/10.1016/j.orggeochem.2016.07.006

Mendoza, P.A., Rajagopalan, B., Clark, M., Cortes, G. and McPhee, J. (2014). A robust multimodel framework for ensemble seasonal hydroclimatic forecasts. Water Resources Research, 50, 6030-6052

Menges, J., Huguet, C., Alcañiz, J.M., Fietz, S., Sachse, D., Rosell-Melé, A. (2014). Influence of water availability in the distributions of branched glycerol dialkyl glycerol tetraether in soils of the Iberian Peninsula. Biogeosciences 11, 2571–2581.

Naafs, B. D. A., Gallego-Sala, A. V., Inglis, G. N., & Pancost, R. D. (2017). Refining the global branched glycerol dialkyl glycerol tetraether (brGDGT) soil temperature calibration. Organic Geochemistry, 106, 48-56.

Peterse, F., J. van Der Meer, S. Schouten, J. W. H. Weijers, N. Fierer, R. B. Jackson, J.-H. Kim, and J. S. Sinninghe Damsté. (2012), Revised calibration of the MBT–CBT paleotemperature proxy based on branched tetraether membrane lipids in surface soils, Geochimica et Cosmochimica Acta, 96, 215–229, doi: 10.1016/j.gca.2012.08.011.

Peterse, F., Martínez-García, A., Zhou, B., Beets, C. J., Prins, M. A., Zheng, H., & Eglinton, T. I. (2014). Molecular records of continental air temperature and monsoon precipitation variability in East Asia spanning the past 130,000 years. Quaternary Science Reviews, 83, 76–82. https://doi.org/10.1016/j.quascirev.2013.11.001

Ravelo, A. C., Dekens, P. S., & McCarthy, M. (2006). Evidence for El Niño-like conditions during the Pliocene. Gsa Today, 16(3), 4.

Regonda, S. K., B. Rajagopalan, M. Clark, and E. Zagona (2006). A multimodel ensemble forecast framework: Application to spring seasonal flows in the Gunnison River Basin. Water Resources Research, 42, W09404, doi:10.1029/2005WR004653

Ropelewski, C. F., & Halpert, M. S. (1987). Global and regional scale precipitation patterns associated with the El Niño/Southern Oscillation. Monthly weather review, 115(8), 1606-1626.

Ropelewski, C. F., & Halpert, M. S. (1989). Precipitation patterns associated with the high index phase of the Southern Oscillation. Journal of climate, 2(3), 268-284.

Russell, J. M., Hopmans, E. C., Loomis, S. E., Liang, J., & Sinninghe Damsté, J. S. (2018). Distributions of 5- and 6-methyl branched glycerol dialkyl glycerol tetraethers (brGDGTs) in East African lake sediment: Effects of temperature, pH, and new lacustrine paleotemperature calibrations. Organic Geochemistry, 117, 56–69. https://doi.org/10.1016/j.orggeochem.2017.12.003

Salzmann, U., A. M. Dolan, A. M. Haywood, W.-L. Chan, J. Voss, D. J. Hill, A. Abe-Ouchi, B. Otto-Bliesner, F. J. Bragg, M. A. Chandler, C. Contoux, H. J. Dowsett, A. Jost, Y. Kamae, G. Lohmann, D. J. Lunt, S. J. Pickering, M. J. Pound, G. Ramstein, N. A. Rosenbloom, L. Sohl, C. Stepanek, H. Ueda, and Z.-s. Zhang. (2013), Challenges in quantifying Pliocene terrestrial warming revealed by data-model discord, Nature Climate Change, 3, 969–974.

Sarachik, E. S., & Cane, M. A. (2010). The El Niño-Southern Oscillation Phenomenon (p. 369). Cambridge: Cambridge University Press. https://doi. org/10.1017/CBO9780511817496.

Sinninghe Damsté, J. S., E. C. Hopmans, R. D. Pancost, S. Schouten, and J. A. J. Geenevasen. (2000). Newly discovered non-isoprenoid glycerol dialkyl glycerol tetraether lipids in sediments. J. Chem. Soc. Chem. Commun. 2000: 1683–1684.

Sinninghe Damsté, J. S., Rijpstra, W. I. C., Hopmans, E. C., Weijers, J. W. H., Foesel, B. U., Overmann, J., & Dedysh, S. N. (2011). 13,16-Dimethyl Octacosanedioic Acid (iso -Diabolic Acid), a Common Membrane-Spanning Lipid of Acidobacteria Subdivisions 1 and 3 . Applied and Environmental Microbiology, 77(12), 4147–4154. https://doi.org/10.1128/aem.00466-11

Sinninghe Damsté, J. S., Rijpstra, W. I. C., Foesel, B. U.,Huber, K.J., Overmann, J., Nakagawa, S., Kim, J.J., Dunfield, P.F., Dedysh, S.N. and Villanueva, L. (2018). An overview of the occurrence of ether- and ester-linked iso-diabolic acid membrane lipids in microbial cultures of the Acidobacteria: Implications for brGDGT paleoproxies for temperature and pH. Organic Geochemistry, 124, pp.63-76. https://doi.org/10.1016/j.orggeochem.2018.07.006

Thomas, E.K., Clemens, S.C., Sun, Y., Huang, Y., Prell, W., Chen, G., Liu, Z. and Loomis, S. (2017). Midlatitude land surface temperature impacts the timing and structure of glacial maxima. Geophysical Research Letters, 44(2), pp.984-992.

Trenberth, K. E., Branstator, G. W., Karoly, D., Kumar, A., Lau, N. C., & Ropelewski, C. (1998). Progress during TOGA in understanding and modeling global teleconnections associated with tropical sea surface temperatures. Journal of Geophysical Research: Oceans, 103(C7), 14291-14324.

649 Van der Hammen, T., J. H., Werner, and H. Van Dommelen. (1973). Palynological record of the upheaval
650 of the northern Andes: a study of the Pliocene and Lower Quaternary of the Colombian Eastern
651 Cordillera and the early evolution of its High-Andean biota, Review of Paleobotany and Palynology,
652 16, 1-122.
653 Wang, H., Liu, W., Zhang, C.L. (2014). Dependence of the cyclization of branched tetraethers on soil
654 moisture in alkaline soils from arid-subhumid China: implications for palaeorainfall reconstructions on
655 the Chinese Loess Plateau. Biogeosciences 11, 6755–6768.
656 Wang, H., Liu, W., & Lu, H. (2016). Appraisal of branched glycerol dialkyl glycerol tetraether-based
657 indices for North China. Organic Geochemistry, 98, 118–130.
658 https://doi.org/10.1016/j.orggeochem.2016.05.013
659 Wara, M. W., Ravelo, A. C., & Delaney, M. L. (2005). Permanent El Niño-like conditions during the
660 Pliocene warm period. Science, 309(5735), 758-761.
661 Weber, Y., C. De Jonge, W. I. C. Rijpstra, E. C. Hopmans, A. Stadnitskaia, C. J. Schubert, M. F.
662 Lehmann, J. S. Sinninghe Damsté, and H. Niemann. (2015). Identification and carbon isotope
663 composition of a novel branched GDGT isomer in lake sediments: Evidence for lacustrine branched
664 GDGT production, Geochimica et Cosmochimica Acta, 154, 118–129.
665 Weber, Y., Damsté, J.S.S., Zopfi, J., De Jonge, C., Gilli, A., Schubert, C.J., Lepori, F., Lehmann, M.F. and
666 Niemann, H. (2018). Redox-dependent niche differentiation provides evidence for multiple bacterial
667 sources of glycerol tetraether lipids in lakes. Proceedings of the National Academy of
668 Sciences, 115(43), 10926-10931.
669 Weijers, J.W.H., Schouten, S., Hopmans, E.C., Geenevasen, J.A.J., David, O.R.P., Coleman, J.M.,
670 Pancost, R.D., Sinninghe Damsté, J.S. (2006). Membrane lipids of mesophilic anaerobic bacteria
671 thriving in peats have typical archaeal traits. Environmental Microbiology 8, 648–657.
672 doi:10.1111/j.1462-2920.2005.00941.x
673 Weijers, J. W. H., S. Schouten, J. C. van den Donker, E. C. Hopmans, and J. S. Sinninghe Damsté. (2007).
674 Environmental controls on bacterial tetraether membrane lipid distribution in soils, Geochim.
675 Cosmochim. Acta, 71, 703–713.
676 Weijers, J. W. H., Panoto, E., Bleijswijk, J. Van, Schouten, S., Rijpstra, I. C., Balk, M., … Damsté, J. S. S.
677 (2009). Constraints on the Biological Source (s) of the Orphan Branched Tetraether Membrane
678 Lipids Constraints on the Biological Source (s) of the Orphan Branched Tetraether Membrane Lipids,
679 0451. https://doi.org/10.1080/01490450902937293
680 Wolfe, J. A. (1995). Paleoclimatic estimates from Tertiary leaf assemblages. Annual Review of Earth and
681 Planetary Sciences, *23*(1), 119-142.
682 Yamamoto, Y., Ajioka, T., & Yamamoto, M. (2016). Climate reconstruction based on GDGT-based
683 proxies in a paleosol sequence in Japan: Postdepositional effect on the estimation of air temperature.
684 Quaternary International, 397, 380–391. https://doi.org/10.1016/j.quaint.2014.12.009
685 Yang, H., Pancost, R.D., Dang, X., Zhou, X., Evershed, R.P., Xiao, G., Tang, C., Gao, L., Guo, Z., Xie, S.
686 (2014). Correlations between microbial tetraether lipids and environmental variables in Chinese soils:
687 optimizing the paleo-reconstructions in semi-arid and arid regions. Geochimica et Cosmochimica Acta
688 126, 49–69.
689 Yang, H., Lü, X., Ding, W., Lei, Y., Dang, X., & Xie, S. (2015). The 6-methyl branched tetraethers
690 significantly affect the performance of the methylation index (MBT') in soils from an altitudinal
691 transect at Mount Shennongjia. Organic Geochemistry, 82, 42–53.
692 https://doi.org/10.1016/j.orggeochem.2015.02.003

693 Zachos, J. C., M. Pagani, L. Sloan, E. Thomas, and K. Billups (2001), Trends, rhythms, and aberrations in
694 global climate 65 Ma to Present, Science, 292, 686–693, doi:10.1126/science.1059412.